Stat3 labels a subpopulation of reactive astrocytes required for brain metastasis

Neibla Priego[1], Cátia Monteiro[1], Lucía Zhu[1], Laura Doglio[1], Liliana del Rocío[1], Manon Mulders[1], David Wasilewski[1,§], Elena Martínez-Saez[2,3], Santiago Ramón y Cajal[2,3], Aurelio Hernández-Laín[4], Riccardo Soffietti[5], Coral Fustero[6], Elena Pineiro[6], Valeria Poli[7], Javier A. Menéndez[8,10,11], Joaquim Bosch-Barrera[9,10,11], Manuel Valiente[1,*].

[1]Brain Metastasis Group, Spanish National Cancer Research Center (CNIO), Madrid E28029 (Spain)
[2]Pathology Department, Vall d´Hebron Hospital, Barcelona E08035 (Spain)
[3]Spanish Biomedical Research NetworkCentre in Oncology (CIBERONC) (Spain)
[4]Neuropathology Unit, Hospital Universitario 12 de Octubre Research Institute, Madrid E28041 (Spain)
[5]Neuro-oncology Department, University and City of Health and Science University Hospital of Turin, Turin 10214 (Italy).
[6]Bioinformatics Unit, CNIO, Spanish National Cancer Research Center (CNIO), Madrid E28029 (Spain)
[7]Molecular Biotechnology Center, University of Turin, Turin 10214 (Italy).
[8]ProCURE (Program Against Cancer Therapeutic Resistance), Metabolism and Cancer Group.
[9]Department of Medical Sciences, Medical School, University of Girona.
[10]Catalan Institute of Oncology (ICO).
[11]Girona Biomedical Research Institute (IDIBGI), Girona (Spain).

[§]Current position: Institute of Neuropathology, University Medical Center Hamburg-Eppendorf.

*Corresponding author

Introductory paragraph

The brain microenvironment imposes a particularly intense selective pressure on metastasis initiating cells. Adaptation of metastatic cells to the brain involves the ability to interact with different components of the microenvironment. We describe a subpopulation of reactive astrocytes located in the vicinity of metastatic lesions that activates Stat3 pathway. Targeting Stat3 in this subpopulation of reactive astrocytes impairs the viability of brain metastases from different primary tumor sources even at advanced stages of colonization. Using a safe and orally bioavailable treatment that targets Stat3 we show that patients with established brain metastasis and extracranial disease benefit notably from this therapy, especially in the CNS. Given that brain metastasis imposes significant morbidity and mortality, this experimental treatment could improve survival of treated patients. Our results indicate that adaptation of cancer cells to the brain microenvironment increases their dependency on organ-specific survival mechanisms. Exploiting these vulnerabilities could allow establishing novel personalized therapies based on the location of metastasis regardless of the origin of the primary tumor.

Text

Histological analysis of experimental brain metastasis with different oncogenomic profiles and primary tumor sources (FigS1a) showed specific activation of Stat3 signaling in the surrounding microenvironment (Fig1a). Co-localization with Gfap (Fig1b, FigS1f-g) indicated that the main cellular source of active Stat3 is reactive astrocytes (RA). Although the presence of Stat3 in other components of the reactive brain metastasis microenvironment has been previously probed[1–3], none of them show

as high levels of activity as those detected in RA (FigS1h). Stat3+ RA do not account for all Gfap+ cells but approximately for half of those surrounding established lesions (Fig1d)(% Gfap+/Stat3+ RA: H2030-BrM, 57.09 ± 3.28; B16/F10-BrM, 45.05 ± 5.86; 482N1, 29.89 ± 3.99). 29 brain metastases from lung adenocarcinoma (21 samples), breast adenocarcinoma (6 samples) and melanoma (2 samples) patients obtained through surgical resection (Table 1) allowed confirming this finding in paraffin embedded human tissues (Fig1e-g). 96.5% of these samples were positive for STAT3+ RA, of which 60.7% scored above 1 (Fig1g). Although barely detected in experimental models (Fig1c), human brain metastases have limited numbers of cancer cells with nuclear phosphorylated STAT3 signal (arrows in FigS1i). The importance of STAT3 in the progression of the disease became evident when both compartments (cancer cells and RA) were analyzed respect to survival from the initial diagnosis. High levels of STAT3 (2 or higher) were prognostic of worst outcome only when evaluated in RA (Fig1h-i). These findings suggest that a subpopulation of RA identified by active Stat3 might play a role in the progression of brain metastasis.

In order to test the functional contribution of Stat3+ RA in brain metastasis we breed a conditional mouse model expressing the human GFAP promoter driving a tamoxifen sensitive Cre to target endogenous Stat3 (GFAP-Cre/ERT2; $Stat3^{loxP/loxP}$, for brevity cKO-Stat3)[4,5]. Newly developed melanoma (FigS1a-e) and previously established lung adenocarcinoma[6] (FigS1a) syngeneic brain metastasis models were used. These brain tropic syngeneic models gained access to this organ without decreasing their aggressive extracranial metastatic potential[6] (FigS1b-e). Brain metastatic (BrM) derivatives were inoculated in the arterial circulation of cKO-Stat3 mice receiving or not tamoxifen and evaluated two weeks later (Fig2a). In order to analyze the effect of targeting Stat3 in RA once brain metastases have developed, we cultured *ex vivo*[6] cKO-Stat3 brain slices containing 2 weeks old lesions grown in mice (Fig2h). A significant decrease in brain tumor burden was detected with bioluminescence imaging (BLI) in cKO-Stat3 treated with tamoxifen *in vivo* (Fig2b-e)(B16/F10-BrM: BLI mean fold increase: 525.02 ± 196.60 cKO-Stat3 untreated, 39.93 ± 14.71 cKO-Stat3 Tmx treated, n= 29 brains per condition) and in organotypic cultures *ex vivo* (Fig2i-j,S2f)(B16/F10-BrM BLI mean fold increase: 6.86 ± 1.57 cKO-Stat3 untreated, 1.30 ± 0.47 cKO-Stat3 4OH-Tmx treated, n≥ 8 brain slices per condition; 482N1 BLI mean fold increase: 2.21 ± 0.52 cKO-Stat3 untreated, 0.37 ± 0.06 cKO-Stat3 4OH-Tmx treated, n≥ 4 brain slices per condition). Effective targeting of Stat3 (FigS2a-b,g) and its consequences were both confirmed with histology (Fig2f-g,S2c). Decreased brain metastasis burden correlated with reduced cancer cell proliferation and increased cancer cell death in organotypic cultures (FigS2g-i). These results suggest a strong dependency of brain metastasis on a pro-metastatic microenvironment regulated by Stat3+ RA. Stat3 has been previously shown to be important in brain metastasis[1,2,7]. However efforts targeting Stat3 in cancer cells[7] did not mimic stronger phenotypes generated with pharmacological approaches[1,2]. By comparing side-by-side genetic and pharmacologic experiments we concluded that targeting Stat3 in RA recapitulates the phenotype obtained with the Stat3 inhibitor WP1066[2] (Fig2h-j). In contrast targeting STAT3 in cancer cells did not entirely reproduce the effects of WP1066 (Fig2k-m,S2j). Activation of Stat3 signaling in reactive astrocytes has been reported in CNS disorders including acute traumatic injury, ischemia, neurodegenerative and autoimmune diseases[8–12], which is suggestive of an innate response to injury that characterizes this organ. Given the absence of Stat3 signaling in Gfap+ reactive astrocytes surrounding brain metastasis initiating cells at early stages of colonization, but their abundance later on surrounding well developed lesions (Fig3a), we hypothesized that Stat3 would become activated once a significant damage and cytokine concentrations had been produced by growing metastatic lesions. To test this hypothesis we added conditioned media (CM) from various BrM cell lines to primary astrocytes (Fig3b). Although we did not detect major changes in astrocytes cultured under standard *in vitro* conditions (data not shown), significant differences emerged when plated under low attachment

conditions. Astrocytes incubated with CM from BrM cells were able to form more numerous and bigger astrospheres in a Stat3 dependent manner (Fig3c-d and data not shown). It was previously shown that the ability to generate spheres was not exclusive of neural stem cells but that mature astrocytes could do it in the absence of tumor suppressors and after stimulation with specific cytokines[13]. Stat3 activating cytokines were frequently upregulated in a broad collection of BrM cancer cell lines, in which three of them (*Egf, Tgfα* and *Mif*) were ubiquitously represented (Fig3e). Incubation of primary astrocytes with a cytokine cocktail including these three cytokines induced the formation of astrospheres in a Stat3 dependent manner (Fig3f-i). cKO-Stat3 derived astrocytes were unable to generate astrospheres when induced by the cytokine cocktail in the presence of 4OH-tamoxifen (Fig3j-k). Astrosphere formation has been previously suggested to reflect a less differentiated state[13] and Stat3+ RA have been recently shown to provide regenerative potential after acute injury[14]. Interestingly the neural stem cell marker Nestin was enriched in Stat3+ astrospheres (FigS3a) as well as in Stat3+ RA associated with brain metastasis (FigS3b-c). These findings suggest that the emerging heterogeneity in surrounding astrocytes could have important functional implications in the context of brain metastasis. In fact reactive astrocytes in brain metastasis have been shown to be anti-metastatic during the initial stages of colonization[6] and pro-metastatic later on[15], a behavior reflecting the complexity of this glial component[16]. To validate the presence of a Stat3 dependent genetic program in brain metastasis associated RA we analyzed Stat3 downstream genes[14] in different experimental models. We confirmed the presence of several Stat3 induced genes in the reactive microenvironment of three different human brain metastasis xenografts (Fig3l-m), some of which were validated *in situ* in reactive astrocytes (Fig3r-s, FigS3d). These genes were also enriched in Stat3+ astrospheres (Fig3n-o), and decreased in cKO-Stat3 brains after the induction of Cre recombinase (Fig3p-q). STAT3 downstream target ICAM1 was validated in reactive astrocytes surrounding human brain metastasis (Fig3t, FigS3e). Experimental and human brain metastases are infiltrated with lymphocytes[17] (FigS3f). We hypothesized that, given the well-established role of Stat3 as an immune regulatory molecule[18,19] and the link between regenerative potential and immunosupression[20–22], Stat3+ RA dependent pro-metastatic functions could include the blockade of anti-tumor activities. We tested this hypothesis incubating activated T cells[23] with conditioned media from Stat3+ astrospheres (FigS3g). This experiment showed that the secretome of Stat3+ RA is sufficient to impair the activation state of lymphocytes[24] (FigS3h-j). Since targeting of Stat3 also impairs brain metastasis viability in T cell depleted animals[1] (Fig2m, Fig4g) additional pro-metastatic roles of Stat3+ RA might exist. Reactive astrocytes surround established brain metastasis without infiltrating the lesion (Fig1b, FigS1g, S3k) reminding a glial scar[9]. However microglia/ macrophages, although enriched at the margins of the lesion, are also found intermingled with highly packed cancer cells at the lesion core[6,25] (FigS3k-l). We found that Iba1+ microglia/ macrophages infiltrating the lesion are enriched in Cd74 (FigS3k). Cd74+ microglia/ macrophages have been shown to promote tumor growth blocking anti-tumor responses derived from microglia/ macrophages[26]. We found that in cKO-Stat3 brains treated with tamoxifen there are less Cd74+/Iba1+ cells infiltrating metastasis (FigS3l-m). Complementary we evaluated the potential influence of Stat3+ astrospheres on Cd74+/Iba1+ cells by incubating wild type brain slices with astrosphere CM during 3 days (FigS3n). Interestingly we observed that this microglia/ macrophage population increased only in the presence of Stat3+ CM (FigS3o-p). Thus the pro-metastatic role of Stat3+ RA could involve the ability to influence various components of the immune system.

We previously reported specific clinical activity of silibinin supplementation against refractory brain metastases in two lung adenocarcinoma patients[27]. Silibinin has been shown to cross the blood-brain barrier[28] and to impair Stat3 activation, although its specific inhibitory mechanism is not known[29]. Consequently we evaluated whether

silibinin exerts its specific effect on brain metastasis by targeting Stat3 signaling in reactive astrocytes. Interestingly silibinin impaired the formation of Stat3+ astrospheres (Fig4a-b). Silibinin also decreased Stat3 activity in the microenvironment surrounding established brain metastasis in organotypic cultures which compromised the viability of Luciferase+ cancer cells (Fig4c-g,FigS4b-c). BrM cell lines used in these experiments were not sensitive to silibinin when treated *in vitro* (FigS4a). *In vivo* treatment of B16/F10-BrM brain metastasis with silibinin (Fig4h) reproduced *ex vivo* results inducing a decrease in brain metastasis burden, as scored by BLI (Fig4i-j) and histology (Fig4k-l), and impaired Stat3 signaling in the microenvironment (Fig4k). Interestingly there was no difference between treated and untreated animals with respect to extracranial metastases (FigS3d-e). Encouraged by these results, the lack of toxicity of silibinin and its oral bioavailability[27,29] we decided to use Legasil®, a commercially available silibinin-based nutraceutical, under compassionate use in an larger cohort of 18 lung cancer patients with brain metastasis. Patients had different histologies and oncogenomic profiles (Table 2) and had been previously treated with WBRT and one of more lines of systemic therapy (Table 3). Noteworthy, three patients who started to take Legasil® under palliative care showed CNS response (Fig4m) and improved their general status, which allowed them to re-initiate additional chemotherapy protocols. Patients were maintained on Legasil® even in combination with chemotherapy. While under Legasil® and additional lines of chemotherapy many patients started or continue to progress extracranially (including primary tumor and metastases out of the brain), their clinical status did not worsen as long as brain metastases continue to respond (Fig4m, FigS4f). From six patients who showed local progression in the brain, four developed new single or multiple brain micro-metastasis that remained below 1 cm and did not generate edema (FigS4g). Overall response rate (ORR) in the brain was higher than extracranially (75.5% vs 40%, p=0.0079) (Fig4n, FigS4h) and included complete response observed in 3 patients (20%) and partial response in 10 patients (55%). Most of the patients ended up progressing outside the CNS. At data cutoff (May 27th, 2017), 5 (27.8%) patients remained alive (12.1-22 months after being diagnosed with brain metastases) (FigS4f). Overall survival (OS) from diagnosis of brain metastasis was significantly superior compared with expected OS calculated by Lung-molGPA (brain GPA Index)[30] (median Legasil®: 22.8 months [95% CI 10.7-35] vs Controls: 6.9 months [4.2-9.6]; p=0·001) (Fig4o). We propose that brain metastatic cells induce and maintain the co-option of a regenerative program driven by Stat3 in a subpopulation of RA, which benefit disease progression by modulating potential anti-tumor responses from the microenvironment. Targeting Stat3+ RA impairs the viability of established brain metastasis in mice and human even at advanced stages of the disease. Based on these results a clinical trial will be initiated.

ONLINE METHODS

Animal Studies

All animal experiments were performed in accordance with a protocol approved by the CNIO, Instituto de Salud Carlos III and Comunidad de Madrid Institutional Animal Care and Use Committee. Athymic nu/nu (Harlan), and C57BL/6 mice 4–6 weeks of age were used. cKO-Stat3 was generated by breeding GFAP-CRE/ERT2 (B6.Cg-Tg(GFAP-cre/ERT2)505Fmv/J, Jackson Labs, ref. 012849) with Stat3loxP/loxP[5]. Brain metastatic derivative of a syngeneic B16/F10 model (B16/F10-BrM) was established according to a previous protocol[31,32]. Brain colonization assays were performed injecting 100 µl of PBS into the left ventricle containing 100,000 cancer cells. Brain colonization was analyzed *in vivo* and *ex vivo* by bioluminescence imaging. Anesthetized mice (Isofluorane) were injected retro-orbitally with D-Luciferin (150 mg/kg) and imaged with an IVIS Spectrum Xenogen machine (Caliper Life Sciences). Bioluminescence analysis was performed using Living Image software, version 3. *Ex vivo* values at the endpoint were normalized to the BLI values of the head in vivo before

starting treating with Tamoxifen (I.p., 1 mg/day) three days after injection of the cancer cells. Tamoxifen was administered until the end of the experiment. Silibinin in the formula of Legasil® was administered by oral gavage daily the same day cancer cells were inoculated (200mg/kg) and until mice reached the endpoint of the experimet.

Brain Slice Assays

Organotypic slice cultures from adult mouse brain were prepared as previously described[6]. Organotypic cultures also included brains obtained at the endpoint of metastatic disease (5-7 weeks in human BrM models, 2 weeks in mouse BrM models), when brain lesions are established. In brief brains were dissected in Hank's balanced salt solution (HBSS) supplemented with HEPES (pH 7.4, 2.5 mM), D-glucose (30 mM), CaCl2 (1 mM), MgSO4 (1 mM), NaHCO3 (4 mM), and embedded in low-melting agarose (Lonza) preheated at 42º C. The embedded brains were cut into 250 µm slices using a vibratome (Leica). Slices were divided at the hemisphere into two pieces. Brain slices were placed with flat spatulas on top of 0.8 µm pore membranes (Millipore) floating on slice culture media (Dulbecco's modified Eagle's medium [DMEM], supplemented HBSS, fetal bovine serum 5%, L-glutamine (1 mM), 100 IU/ml penicillin, 100 mg/ml streptomycin). Brain slices were imaged to confirm the presence of established metastases using BLI. If brain slices receive a treatment, BLI was acquired 12h after plating (Day 0) and 4 days after the addition of the inhibitor (Day 5). Growth rate was obtained by comparing fold increases between day 5 and day 0. Treatments to brain slices were given once during the experiment (4OH-Tmx, 1 µM, Sigma-Aldrich, ref. H7904; WP1066, 10 µM, Merck, ref. 573097; Doxycycline, 1 µg/ml, Sigma-Aldrich, ref. D9891; silibinin, 100 µM, Sigma-Aldrich, ref. S0417) by adding them to the media.If inhibitors were added to wild type mice where recombination was not necessary, slices were incubated 3 days. If slices were obtained from brains without metastases $3x10^4$ cancer cells suspended in 2 µl of culture media were placed on the surface of the slice and incubated for 3 days. BrdU pulse (0.2 mg/ml, Sigma-Aldrich, ref. B9285) was given by adding it in the media four hours before fixation. Brain slices were fixed in paraformaldehyde (4%) overnight, and then free-floating immunofluorescence was performed. Slices were mounted with Mowiol-Dabco anti-fade reagent. Analysis of the knockdown level in H2030-BrM (Figure S2S) was analyzed in a homogenate containing the mouse brain tissue and human cancer cells. Use of human primers allowed to evaluate *STAT3*.

Cell culture

Human and mouse brain metastatic cell lines were previously described[6,31–33]. B16/F10-P cells were injected intracardiacally to obtain brain metastatic derivatives. Briefly, a cell suspension containing 10^5 B16/F10-P cells expressing a Luciferase construct (Addgene ref. 19166, Blasticidine resistance)[34], in a volume of 100 µl was injected in the left cardiac ventricle of anesthetized 4–6 week-old C57BL/6 mice. Tumor development was monitored by weekly bioluminescence imaging using the IVIS-200 imaging system. Brain lesions were localized by *ex vivo* bioluminescence imaging, and resected under sterile conditions. Tissue was minced and placed in culture medium containing a 1:1 mixture of DMEM/Ham's F12 supplemented with 0.125% collagenase III and 0.1% hyaluronidase. Samples were incubated at 37º C for 1 h, with gentle rocking. After collagenase treatment, cells were briefly centrifuged, resuspended in 0.25% trypsin, and incubated at 37º C for 15 min. Cells were resuspended in culture media and allowed to grow to confluence on a 10 cm dish. Two additional rounds of *in vivo* selection were performed. Brain metastatic cells (BrM3) were fluorescently labelled with a lentiviral vector encoding ZsGFP and sorted for further propagation in culture or inoculation in mice.

MDA231-BrM2 (abbreviated as MDA231-BrM), ErbB2-BrM2 (abbreviated as ErbB2-BrM), 373N1, 393N1, 482N1, 2691N1, B16/F10-BrM3 (abbreviated as B16/F10-BrM) where cultured in DMEM media supplemented with 10% fetal bovine serum (FBS), 2 mM L-Glutamine, 100IU/ml penicillin/streptomycin and 1 mg/ml amphotericin B.

H2030-BrM3 (abbreviated as H2030-BrM), PC9-BrM3 (abbreviated as PC9-BrM) and HCC1954-BrM1a (abbreviated as Hcc1954-BrM) were cultured in RPMI1640 media supplemented with 10% fetal bovine serum (FBS), 2 mM L-Glutamine, 100IU/ml penicillin/streptomycin, and 1 mg/ml amphotericin B. For lentivirus production, 293T cells were cultured in DMEM media supplemented with 10% fetal bovine serum (FBS), 2 mM L-Glutamine, 100 IU/ml penicillin/streptomycin, and 1 mg/ml amphotericin B. Mouse astrocytes were obtained from one to three day old pups[35]. In brief, brains were mechanically dissociated, filtered through 100 mm filters and cell suspension cultured in a petri dish during the next 7 days. On day 7, the dish was incubated overnight at 37º C with gentle shaking. Next day media was changed and astrocyte enrichment confirmed with > 90% of cells staining positive for GFAP.

T-cells in vitro experiments

T-cells were obtained from the spleen of 10-15 week-old C57BL/6 mice. T cells were sorted using anti-mouse CD8a-FITC (Tonbo Biosciences, ref.35-008-1, 1:200), anti-mouse NK1.1-PE (e-Bioscience, ref. 12-5941-82, 1:200) and anti-mouse CD11C-APC (BD Biosciences ref. 550261, 1:200) and activated with anti-mouse CD3e clone 145-2C11 (BD Biosciences ref. 553066, 1:200) coated plates, soluble anti-mouse CD28 (37.51) (1µg/ml; Tonbo Biosciences, ref. 70-0281-U500) and mouse IL2 (1 µg/ml; Miltenyi Biotec, ref. 130-094-054). CD8+ CD11C- NK1.1- cells were cultured in RPMI medium supplemented with 10% FBS and Penicillin-Streptomycin for one day and then the conditioned media from astrospheres was added to the culture. After 2 days, flow cytometry analysis was performed using the following antibodies: CD62-L-APCR700 (BD Biosciences, ref. 565159, 1:200), CD44-PE (BD Biosciences, ref. 553134, 1:200) and CD25-PerCP-Cyanine5.5 (e-Bioscience, ref. 45-0251-80, 1:200) in the FACSCalibur flow cytometer (BD Biosciences). Data was analyzed using FlowJo software.

qRT-PCR

Whole RNA was isolated using RNAeasy Mini Kit (QIAGEN). 1000 ng RNA was used to generate cDNA using iScript cDNA Synthesis Kit (Bio-Rad, ref. 1708890). RNA obtained from mouse brains included microdissected established metastases from human BrM cells, in which the microenvironment was analyzed by using mouse primers, and microdissected BrM metastases that had grown in cKO-Stat3 brains treated or not with Tmx. In this case the microenvironment was separated by dissecting Luciferase- tissue immediately adjacent to Luciferase+ cancer cells. Microdissection in cKO-Stat3 was initially validated by confirming the absence of Gfp+ cell using flow cytometry (data not shown). RNA from BrM cell lines was obtained from a confluent well from a 6 well plate. RNA from astrospheres was obtained from cells cultured in 24 well plates or 10 cm plates, both low attachment. Gene expression was analyzed using SYBR green gene expression assays (GoTaq® qPCR Master Mix Promega, ref. A6002).

Primers used for human genes (5´->3´, forward;reverse):

-*STAT3* (CTGAGCTGGCAGTTCTCCTC; GAAGGTGCCTGGAGGCTTAG).

Primers used for mouse genes (5´->3´, forward;reverse):

-*Stat3* (CAGAAAGTGTCCTACAAGGGCG;CGTTGTTAGACTCCTCCATGTTC),

-*Gfap* (ACGTTAAGCTAGCCCTGGAC;GGTGAGCCTGTATTGGGACAA),

-*Icam1* (TTTGAGCTGAGCGAGATCGG;AGAGGTCTCAGCTCCACACT),

-*Ctgf* (GTGCCAGAACGCACACTG;CCCCGGTTACACTCCAAA),

-*Timp1* (GAGACACACCAGAGCAGATACC;TGGTCTCGTTGATTTCTGGGG);

-*Pdl1* (TTCACAGCCTGCTGTCACTT;CTCTCCCCCTGAAGTTGCTG),

-*Lcn2* (GAACTTGATCCCTGCCCCAT;TTCTGATCCAGTAGCGACAGC),

-*Ptx3* (CTTCCCAATGCGTTCGAAGAAGATTTTTGG;AACACTTAAGAAACATACTGGGCTCCTCCG),

-*Dnmt3a* (GCCGAATTGTGTCTTGGTGGATGACA;CCTGGTGGAATGCACTGCAGAAGGA),

-*Vegfa* (CCTGGCCCTCAAGTACACCTT;TCCGTACGACGCATTTCTAG),
-*Tgfβ1* (CTGCTGACCCCCACTGATAC;GTGAGCGCTGAATCGAAAGC),
-*Mif* (CTTTGTACCGTCCTCCGGTC;CGTTCGTGCCGCTAAAAGTC).
Relative gene expression was normalized to the ‘‘housekeeping’’:
Human genes (5´->3´, forward;reverse):
-*B2M* (AGATGAGTATGCCTGCCGTG;TCATCCAATCCAAATGCGGC).
Mouse genes (5´->3´, forward;reverse):
-Actin (GGCACCACACCTTCTACAATG;GTGGTGGTGAAGCTGTAGCC-3´).
Quantitative PCR reaction was performed on QuantStudio 6 Flex Real-Time PCR System (Applied Biosystems) and analyzed using the software QuantStudio 6 and 7 Flex Software.

Clinical samples and immunohistochemistry

29 cases from lung cancer (21 cases), breast cancer (6 cases) and melanoma (2 cases) brain metastasis were obtained from the Department of Pathology, Vall d´Hebron Hospital and the Department of Pathology, Hospital 12 de Octubre after confirming they belong to surgeries were extended resection was performed, which was necessary to evaluate the surrounding microenvironment. Paraffin embedded tissues were obtained in compliance with protocols approved by Hospital Val d´Hebron, Hospital 12 de Octubre and University Hospital of Turin Institutional Review Board (IRB). Immunohistochemistry for GFAP (Ventana Medical Biosystem, ref. 760-4345), STAT3 (Tyr705) (Cell Signaling, ref. 9145, 1:100), ICAM1 (Sigma-Aldrich, ref. HPA004877, 1:500), were performed by the Vall d´Hebron Hospital and CNIO Histopathology Core Facility using standardized automated protocols. Stainings were evaluated and scored by clinical pathologists (E.M.S., S.R.C) in a blinded fashion. 16 samples had annotated clinical history related to time to death from diagnosis of the primary tumor.

Immunofluorescence and immunohistochemistry

Tissue for immunofluorescence was obtained after overnight fixation with PFA 4% at 4 C. Slicing of the brain was done by using a vibratome (Leica) or sliding microtome (Fisher). Both types of brain slices (250 µm and 80 µm respectively) were blocked in NGS 10%, BSA 2%, Triton 0.25% in PBS for 2 hr at room temperature (RT). Primary antibodies were incubated overnight at 4C in the blocking solution and the following day for 30 min at RT. After extensive washing in PBS-Triton 0.25%, the secondary antibody was added in the blocking solution and incubated for 2 hr. After extensive washing in PBS-Triton 0.25%, nuclei were stained with Bis-Benzamide (1 mg/ml; Sigma) for 7 min at RT. Primary antibodies: GFP (Aves Labs, ref. GFP-1020, 1:1,000), Stat3 (Tyr705) (Cell Signaling, ref. 9145, 1:100), GFAP (Millipore, ref. MAB360, 1:1000), Iba1 (Wako, ref. 019-19741, 1:500), Nestin (BD Bioscience, ref. 556309, 1:100), NeuN (Millipore, ref. MAB377, 1:500), cleaved caspase-3 (1:500, ref. 9661; Cell Signaling), BrdU (Abcam, ref.ab6326, 1:500), Cd8 (Novus Biologicals, ref. NB200-578, 1:100), Cd74 (BD Biosciences, ref. 555318, 1:100), Cd31 (BD Pharmingen, ref. 550274, 1:100), Cd68 (KP1) (Abcam, ref. ab955 1:200). Secondary antibodies: Alexa-Fluor anti-chicken488, anti-rabbit555, anti-mouse555, anti-mouse633, anti-mouse647 (Invitrogen, dilution 1:300). Same protocol was applied to stain astrospheres. Brain slices or astrospheres were pre-treated with Methanol 10 minutes at -20 C previous to start the immunofluorescence against phosphorylated Stat3. Immunohistochemistry against Stat3 (Tyr705) (Cell Signaling, ref. 9145, 1:100) was performed in paraffin embedded brain sections (5µm) using standardized automated protocols at the CNIO Histopathology Core Facility.

Quantification and statistics

Data are represented as the mean values ± S.E.M. When comparisons were done between two experimental groups, an unpaired Student's t test was used. Overall survival was calculated by Lung-molGPA tool and Kaplan–Meier survival curves were generated. For survival curves P values were obtained with log rank (Mantel-Cox) test. Heatmaps were generated using Morpheus software

(https://software.broadinstitute.org/morpheus/). For comparatives in cKO-Stat3 and astrospheres a relative scale is used for the representation that takes the minimum and maximum values for each gen. For comparatives in human BrM metastases and BrM cytokines we globally set the minimum as 0 and maximum as 3 and -1.5 and 1.5, respectively, for all the genes.

Astrosphere assays

Mouse astrocytes were treated with conditioned media from BrM cell lines or with recombinant mouse protein including Egf (0.01 µg/ml, R&D Systems, ref. 2028-EG-200), Mif (0.1µg/ml, R&D Systems, ref. 1978-MF-0257CF) and Tgfα (0.1µg/ml, R&D Systems, ref. 239-A-100) during 96 hours. After this treatment 10^4 astrocytes were seeded in low attachment plates and incubated for seven days in the presence of the same media to evaluate the ability to form astrospheres. Conditioned media from BrM cell lines were obtained after 3 days incubation of cancer cells in DMEM supplemented with 0.25 % FBS, 2 mM L-Glutamine, 100IU/ml penicillin/streptomycin and 1 mg/ml amphotericin B. After being collected, the media was filtered and added to astrocytes or stored at -80º C. Conditioned media from astrospheres was collected, filtered and added to activated Cd8 cells (Figure S3h) or wild type brain slices (Figure S3n).

Human patients treated with silibinin

18 individuals with lung cancer and brain metastasis have been treated with Legasil® in the Catalan Institute of Oncology, Hospital Universitari Dr. Josep Trueta of Girona (Spain). Each capsule of Legasil® contains 210 mg of Eurosil 85 (60% of silibinin isoforms). Legasil® (Meda Pharma, Rottapharm-Madaus, Barcelona, Spain) was started at a dose of 2 capsules/day (1-0-1) for 3 days and increased progressively every 3 days to reach up to 5 capsules dosage (1,050 mg of Eurosil85) or until toxicity was observed. Legasil® is available in ambulatory pharmacies of Spain without medical prescription as it is considered a nutritional supplement. All individuals gave written informed consent. The experimental protocol (compassionate treatment with silibinin supplementation) was approved by the Ethics Committee of the Hospital Universitari Dr. Josep Trueta (Girona, Spain). We certify that all applicable institutional regulations concerning the ethical use of information from human patients were followed during this research.

Image acquisition and analysis

Images were acquired with a Leica SP5 up-right confocal microscope 10X, 20X, 40X and 63X objectives and analyzed with ImageJ software. Astrospheres were imaged with Leica DMi1 inverted microscope.

FIGURE LEGENDS

Figure 1. Stat3 labels a subpopulation of reactive astrocytes associated with established brain metastasis independently of the origin of the primary tumor.

a. Immunohistochemistry against phosphorylated Stat3 (Tyr705) in a brain with established H2030-BrM lung adenocarcinoma metastasis. Images correspond to different fields according to the location of the metastasis (i: field of view containing the metastasis; ii: field of view far from the metastasis. Dotted line surrounds cancer cells. Scale bar: 100 µm, high magnification 25 µm. **b.** Immunofluorescence labeling reactive astrocytes (Gfap) and phosphorylated Stat3 (Tyr705) in the area surrounding a metastasis. A subpopulation of reactive astrocytes shows active Stat3. Scale bar: 35 µm. **c.** Stat3+ cells are present in the microenvironment of multiple brain experimental models originated from lung cancer (PC9-BrM, 393N1), breast cancer (Hcc1954-BrM, MDA231-BrM, ErbB2-BrM) and melanoma (B16/F10-BrM). Gfp: Cancer cells (human and mouse origins). High magnifications indicate lack of co-localization of Gfp+ with pStat3 (Tyr705). Scale bar: 50 µm (Hcc1954-BrM, MDA231-BrM, PC9-BrM, ErbB2-BrM), 75 µm (B16/F10-BrM, 393N1), high magnification 10 µm. **d.** Percentage of double labeled Gfap+/ pStat3+ cells. Values indicate mean values ± SEM, 3 metastases were scored in each model. **e.** 29 brain metastases (72% from lung cancer, 21% from breast cancer, 7% from melanoma) were evaluated for GFAP and

pSTAT3 (Tyr705). **f.** Representative image showing pSTAT3+ (Tyr705) reactive astrocytes (RA) surrounding brain metastasis (dotted line). Scale bar: 15 µm. **g.** Quantification of pSTAT3+ RA in human brain metastasis. 28/ 29 (96.5%) showed positive staining of pSTAT3 in RA, from which 4/ 28 (14%) scored with 3, 13/ 28 (46%) with 2 and 11/ 28 (39%) with 1 according to the abundance and signal intensity of pSTAT3 in the microenvironment. **h.** Overall survival from diagnosis of the primary tumor to death was available for 17/ 29 patients. A survival curve was generated grouping patients with high (Score 3 and 2) and low (Score 1 and 0) pSTAT3 in the microenvironment. P values were obtained with log rank (Mantel-Cox) test. **i.** Same patients were used to generate a survival curve according to the same criteria but scoring pSTAT3 in cancer cells. P values obtained with log rank (Mantel-Cox) test.

Figure S1.
a. Experimental brain metastasis models used in this study indicating their primary tumor source, specie of origin and major molecular alterations. Adca: adenocarcinoma, Mel: melanoma. **b,d.** Representative images of wild type C57BL/6 mice two weeks after being inoculated with B16/F10-P or B16/F10-BrM cells intracardiacally. Images showing the BLI of brains (b) and thorax and abdomen (d) *ex vivo* are also shown. Dotted line indicated the body of mice. **c.** Quantification of bioluminescence imaging (BLI) in the area of the head. Error bars, S.E.M. (n=8 mice per experimental condition). P value is calculated using two-tailed t test. **d.** Survival curve comparing B16/F10-P with B16/F10-BrM cell lines. P value is calculated using log rank (Mantel-Cox) test. **f.** High magnification of reactive astrocytes (RA) with activated Stat3 (Tyr705) in brain metastasis models shown in figure 1c. Scale bar: 5 µm. **g.** Double immunofluorescence of an additional brain metastasis model showing co-localization of pStat3 (Tyr705) with reactive astrocytes. Cc: cancer cells. Dotted line: metastasis margins. Scale bar: 50 µm. **h.** Double immunofluorescence of pStat3 (Tyr705) and different components of the microenvironment surrounding brain metastases. All images correspond to the immediate vicinity of a Gfp+ brain metastasis (not shown). Scale bar: 25 µm. **i.** Immunohistochemistry performed in consecutive paraffin sections of a human brain metastasis shows that pSTAT3+ (Tyr705) cells are mostly circumscribed to GFAP+ cells. Arrows point to pSTAT3+ cancer cells.

Figure 2. Genetic targeting of Stat3 in reactive astrocytes impairs the viability of brain metastasis.
a. Schema of experimental design. **b.** Representative images of cKO-Stat3 two weeks after being inoculated with B16/F10-BrM cells intracardiacally. Bioluminescence was analyzed in the area of the head (white line, arrow) comparing animals receiving Tamoxifen (IP, 1mg, daily, 14 doses) with those that did not. **c.** Quantification of bioluminescence imaging (BLI). Every dot represents a different animal. Values were obtained from normalizing *ex vivo* brain signal to *in vivo* head signal 3 days after IC injection when treatment was initiated. Error bars, S.E.M. (n=29 mice per experimental condition, 5 independent experiments). P value is calculated using two-tailed t test. **d.** Images of *ex vivo* brains that represent different categories according to normalized photon flux intensity. **e.** Quantification showing the percentage of mice in each category according to the BLI fold increase values. **f.** Representative images of established metastases at the endpoint of the experiment. High magnification images show pStat3+ (Tyr705) cells in the microenvironment. Dotted line: Gfp+ B16/F10-BrM cancer cells. Scale bar: 100 µm, high magnification 50 µm. **g.** Quantification of the size of metastatic lesions in the cKO-Stat3 in Tamoxifen treated or untreated mice. Error bars, S.E.M. (n=5 and 6 metastases respectively, 2 independent experiments). P value is calculated using two-tailed t test. **h.** Schema of experimental design. 4OH-Tmx or WP1066 were added to cKO-Stat3 brain slices containing established B16/F10-BrM metastases. **i.** Representative wells containing brain organotypic cultures with established B16/F10-BrM metastases grown *ex vivo* during five days in the presence

or absence of 4OH-Tmx (1μM) or WP1066 (10μM). The image shows the bioluminescence intensity in each condition for each brain slice, which indicates the amount of Luciferase+ B16/F10-BrM cells contained in the brain tissue. **j.** Quantification of the bioluminescence signal emitted by B16/F10-BrM cells in each brain slice normalized by the initial value obtained at day 0 (before the addition of either 4OH-Tmx or WP1066). Every dot represents a different organotypic culture. Error bars, S.E.M. (n= 12 control and 8 4OH-Tamoxifen and 8 WP1066 treated organotypic cultures, 2 independent experiments). P value is calculated using two-tailed t test. **k.** Schema of experimental design. Doxycycline (1 μg/ml) or WP1066 (10μM) were added to slices containing established H2030-BrM metastases previously transduced with a Doxycycline inducible shRNA against human *STAT3* (iH2030-BrM sh*STAT3*). BLI was obtained before the addition of either Doxycycline or WP1066 to the media (Day 0). Five days later BLI was performed to analyze metastasis growth *ex vivo* by normalizing BLI values to day0, before the addition of either Doxycycline or WP1066 to the media. **l.** Representative images of brain organotypic cultures with established iH2030-BrM sh*STAT3* metastases grown *ex vivo* during five days in the presence or absence of Doxycycline (1 μg/ml) or WP1066 (10μM). The image shows the bioluminescence of Luciferase+ iH2030-BrM sh*STAT3* cells under different culture conditions. **m.** Quantification of the bioluminescence signal emitted by iH2030-BrM sh*STAT3* cells in each brain slice normalized by the initial value obtained at day 0, before the addition of any treatment. Every dot represents a different organotypic culture. Error bars, S.E.M. (n=4 organotypic cultures per experimental condition). P value is calculated using two-tailed t test.

Figure S2

a. Representative images of Gfp+ B16/F10-BrM metastases scored according to the amount of pStat3 (Tyr705) signal in the surrounding microenvironment. Colored squares on the top-right corner correspond to the quantification in j. Scale bar: 100 μm. **b.** Distribution of B16/F10-BrM metastases according to the associated pStat3 signal in the surrounding microenvironment (n=28 control metastases, 7 tamoxifen treated metastases) comparing Tamoxifen treated and untreated cKO-Stat3 mice. **c.** Quantification of the mean number of Gfp+ B16/F10-BrM brain metastases found in cKO-Stat3 Tamoxifen treated or untreated mice. Error bars, S.E.M. (n=11 brains per experimental condition). P value is calculated using two-tailed t test. **d.** 4OH-Tmx (1μM) treatment of B16/F10-BrM cells *in vitro* does not influence their growth rate measured by bioluminescence signal (Control: n=20; mean bioluminescence fold increase at day 5= 43.06 ± 6.47; 4OH-Tmx: n=19; mean bioluminescence fold increase at day 5= 49.29 ± 7.58). **e.** B16/F10-BrM established brain metastases in wild type mice grown as organotypic cultures in the presence 4OH-Tmx (1μM). Bioluminescence signal was found to be identical to untreated slices (n=4 organotypic cultures per experimental condition; Control: mean bioluminescence fold increase at day 5= 130.24 ± 53.04; 4OH-Tmx: mean bioluminescence fold increase at day 5= 167.74 ± 88.79). **f.** Quantification of the bioluminescence signal emitted by 482N1 established metastases in CKO-Stat3 mice comparing 4OH-Tmx (1μM) treated and untreated cultures. Every dot represents an individual organotypic culture. Error bars, S.E.M. (n=4 organotypic cultures per experimental condition). P value is calculated using two-tailed t test. **g.** Representative images of the histology from the experiment shown in Fig2i. In order to evaluate proliferation and cell death markers the analysis was performed on the limited Gfp+ brain metastases still present in 4OH-Tmx treated brain slices. CC3: cleaved Caspase 3. pStat3 (Tyr705) signal was scored in areas surrounding Gfp+ cells. Scale bar: 250 μm (BrdU), 100 μm (CC3), 75 μm (pStat3). **h.** Quantification of the percentage of BrdU positive cancer cells in cKO-Stat3 organotypic cultures treated with 4OH-Tmx. Error bars, S.E.M. (n=8 field of view from 3 metastases per experimental condition). P value is calculated using two-tailed t test. **i.** Quantification of the percentage of cleaved Caspase 3 positive cancer cells in cKO-

Stat3 organotypic cultures treated with 4OH-Tmx. Error bars, S.E.M. (n=4 field of view from 2 metastases per experimental condition). P value is calculated using two-tailed t test. **j.** qRT-PCR against human *STAT3* was performed on brain slices shown in fig2l-m after being cultured for five days in the presence or absence of Doxycycline.

Figure 3. *De novo* induced Stat3 activity confers a differential functional identity to reactive astrocytes.

a. Immunofluorescence against pStat3 (Tyr705) and reactive astrocytes at early (1 week) and advances stages (6 weeks) during brain colonization. pStat3+ reactive astrocytes are not present at earlier time-points. Scale bar: 50 μm, high magnification4 μm. **b.** Schema of experimental design. The formation of astrospheres was analyzed after incubation of primary astrocytes with conditioned media (CM) from brain metastatic (BrM) cells. **c.** Representative images of astrospheres incubated with and without BrM CM. More and bigger astrospheres were found when incubated with BrM CM. Scale bar: 1 mm. **d.** Quantification of the size of astrospheres induced by the CM of H2030-BrM cell line. Error bars, S.E.M. (n=10 wells control, 8 wells CM H2030-BrM, 3 wells H2030-BrM with WP1066). P value is calculated using two-tailed t test. **e.** Heatmap indicating human or mouse Stat3 activating cytokines scored in multiple BrM cell lines by qRT-PCR. Level of each cytokine was evaluated in three independent experiments relative to their parental non-brain tropic cell lines. **f.** Schema of experimental design. A cocktail of three cytokines was used to evaluate their ability to induce astrospheres. **g.** Representative images showing astrospheres formed under different experimental conditions. High magnification shows pStat3 (Tyr705) in astrospheres. WP1066 impairs the formation of astrospheres in the presence of the cytokine cocktail. Scale bar: 2 mm, high magnification 100 μm. **h.** Quantification of the experiment in g. Error bars, S.E.M. (n≥6 wells per condition). P value is calculated using two-tailed t test. **i.** Quantification of pStat3+ cells in astrospheres from experiment in g. Error bars, S.E.M. (n≥6 wells per experimental condition). **j.** Representative images of cKO-Stat3 derived astrospheres that were generated in the presence or absence of 4OH-Tamoxifen (1μM) and a cytokine cocktail as in shown in f. Scale bar: 2 mm, high magnification 100 μm. **k.** Quantification of the experiment in j. Error bars, S.E.M. (n=4 wells per condition). P value is calculated using two-tailed t test. **l.** Schema of experimental design. Established metastases from human BrM cell lines were dissected along with the surrounding mouse microenvironment to obtain RNA and perform qRT-PCR. **m.** Heatmap of mouse genes in the microenvironment surrounding resected metastases. Wild type corresponds to a brain without metastases. Values were obtained from analysis of three different resected metastases for each BrM cell line. **n.** Schema of experimental design. Astrospheres generated in the presence of a cytokine cocktail (as in f) and the Stat3 inhibitor WP1066 were used to evaluate Stat3 downstream genes. **o.** Heatmap showing Stat3 downstream genes differentially expressed in astrospheres treated with the cytokine cocktail as described in f. Values were obtained from the analysis of six independent experiments. **p.** Schema of experimental design. Brains from Tamoxifen treated and untreated cKO-Stat3 mice were obtained two weeks after IC injection of B16/F10-BrM cells. Lesions were microdissected *ex vivo* and Luciferase (-) tissue (2) was processed to perform qRT-PCR analysis. **q.** Heatmap showing upregulation of Stat3 downstream genes in the microenvironment associated with B16/F10-BrM metastases and their downregulation in brains from cKO-Stat3 mice treated with Tamoxifen (Tmx). Values were obtained from the analysis of ten brains per condition. Control values were obtained from the use of five cKO-Stat3 brains from mice not injected with BrM cells. **r-s.** Double immunofluorescence of Stat3 downstream genes. Icam1 co-localizes with pStat3 (Tyr705) (r) and Ctgf with Gfap (s). White arrows indicate double positive cells. Dotted lines surround established metastases. Cc: cancer cells, labelled in blue (r) or green (s) by Gfp immunofluorescence. Scale bar: 25 μm. **t.** Immunohistochemistry of ICAM1 in human brain metastases samples. ICAM1 was found in the majority of

samples in reactive astrocytes (FigS4e). High magnification shows ICAM1+ cell morphology compatible with a reactive astrocyte in the vicinity of cancer cells. Cc: cancer cells. Scale bar: 100µm, high magnification 25µm.

Figure S3

a. Astrospheres generated in the presence of the cytokine cocktail are positive for Nestin. Scale bar: 250 µm. **b-c.** Nestin+ reactive astrocytes surround established brain metastases (b) and co-localize with Stat3 (Tyr705) (c). Cc: cancer cells, B16-F10-BrM (b) and H2030-BrM (c). Scale bar: 100 µm (b, low magnification), 10 µm (b, high magnification and c). **d.** Double immunofluorescence of Stat3 downstream genes. Pd-l1 co-localizes with Gfap. White arrows indicate double positive cells. Dotted lines surround established metastases. Cc: cancer cells, labeled in green. Scale bar: 75 µm (low magnification), 25 µm (high magnification). **e.** Percentage of 23 human brain metastases with ICAM1 positive staining in reactive astrocytes and their immunohistochemistry score. **f.** Immunofluorescence against Cd8 in established brain metastasis from mouse BrM experimental models (see FigS1a). Scale bar: 12 µm. **g.** Schema of experimental design. Näive Cd8 T cells obtained from C57B/6 wild type mice were activated *in vitro* before being incubated with conditioned media (CM) from astrospheres during 48 hours and later analyzed by flow cytometry. **h.** Flow cytometry of pre-activated Cd8 lymphocytes after being incubated with the conditioned media generated by Stat3- and Stat3+ astrospheres. Relative presence of Cd25, Cd62l and Cd44 surface markers in T cells were differentially influenced by the secretome of astrospheres. **i-j.** Quantification of experiments shown in h. Error bars, S.E.M. (n=3 co-cultures per experimental condition). P value is calculated using two-tailed t test. **k.** Double immunofluorescence of Gfap+ reactive astrocytes and Cd74+ macrophages/ microglia in an established brain metastasis. Only Cd74+ cells infiltrate the lesion. Cancer cells are in blue (Gfp). Scale bar: 50 µm. **l.** Representative images of established metastases where Iba1+ and Cd74+ cells are labeled. Cancer cells are in blue (Gfp). White arrows label double positive Iba1+/Cd74+ cells inside the metastasis, while grey arrows label those surrounding the metastasis. Scale bar: 75 µm. **m.** Quantification of the experiment shown in l. Error bars, S.E.M. (Control: n=11 field of view, from 4 metastases, 2 brains; Tamoxifen: n=8 field of view, from 4 metastases, 3 brains). P value is calculated using two-tailed t test. **n.** Schema of experimental design. CM: conditioned media from astrospheres. **o.** Wild type brain slices incubated with conditioned media from Stat3- or Stat3+ astrospheres and Cd74+/Iba1+ cells labeled. Scale bar: 50 µm. **p.** Quantification of the experiment in n. Error bars, S.E.M. (Control: n=12 field of view, from 2 organotypic cultures; 4OH-Tmx: n=14 field of view, from 2 organotypic cultures). P value is calculated using two-tailed t test.

Figure 4. Targeting Stat3+ reactive astrocytes pharmacologically impairs the viability of brain metastasis in mice and human.

a. Representative images of astrospheres treated with the cytokine cocktail (Egf, Mif, Tgfα) in the absence or presence of silibinin (100 µM). Scale bar: 2 mm. **b.** Quantification of the experiment shown in (a). Error bars, S.E.M. (n=4 wells per experimental condition). P value is calculated using two-tailed t test. **c.** Schema of experimental design. Wt: wild type. **d,f.** Representative images of brain organotypic cultures with B16/F10-BrM (d) or H2030-BrM (f) established metastases that were grown *ex vivo* during three days in the presence or absence of silibinin (100 µM). pStat3 (Tyr705) immunofluorescence in the surrounding microenvironment is also shown. Scale bar: 35 µm. **e,g.** Quantification of the experiment shown in (d) and (f). Error bars, S.E.M. (n=5-12 organotypic cultures per experimental condition). P value is calculated using two-tailed t test. **h.** Schema of experimental design. Silibinin was administered by oral gavage (o.g.) daily during two weeks. **i.** Representative bioluminescence images of control and silibinin treated animals at the endpoint of the experiment. E*x vivo* brain bioluminescence is also shown. **j.** Quantification of the

experiment shown in (i). Error bars, S.E.M. (Control: n=8 brains; silibinin: n=9 brains). P value is calculated using two-tailed t test. **k.** Representative images of metastases found in silibinin treated and untreated brains. Dotted line surrounds metastases. Cc: cancer cells. Scale bar: 25 μm. **l.** Quantification of the experiment shown in (k). Error bars, S.E.M. (Control: n=8 brains; silibinin: n=9 brains). P value is calculated using two-tailed t test. **m.** Sequential intracranial (metastasis) and thoracic (primary tumor) MRI of one patient treated with silibinin. Images shown were taken immediately before initiating silibinin treatment (pre-silibinin) under palliative care and sixteen months later. During this time the patient received silibinin and additional chemotherapy lines. **n.** Intracranial overall response rate (ORR) waterfall of 17 patients with lung cancer brain metastases who received silibinin under compassionate use. Dotted grey line indicates 30% reduction of metastases. One patient was excluded from the waterfall plot because death ocurred before the first control brain MRI could be performed. Asterisks indicate patients who receive silibinin under palliative care. **o.** Overall survival (OS) from diagnosis of brain metastasis of 18 patients who received silibinin compared to OS of the same patients calculated by Lung-molGPA tool (brain GPA Index[30]) Kaplan–Meier survival curves were generated. P value is calculated by log-rank test.

Figure S4

a. Representative bioluminescence images and quantification of various BrM cell lines cultured *in vitro* in the absence or presence of silibinin (100 μM) during 3 days. Dots are independent replicas. Dotted line indicates the mean value. P value is calculated using two-tailed t test. **b.** Representative images of brain organotypic cultures with 482N1 established metastases grown *ex vivo* during three days in the presence or absence of silibinin (100 μM). **c.** Quantification of the experiment shown in (b) (n=7 organotypic cultures per condition). P value is calculated using two-tailed t test. **d.** Representative bioluminescence *ex vivo* images of the thorax and abdomen of experiment shown in 4i. **e.** Quantification of the experiment shown in (d). Error bars, S.E.M. (Control: n=8 mice; silibinin: n=9 mice). P value is calculated using two-tailed t test. **f.** Clinical progression of 18 patients treated with silibinin from diagnosis of the brain metastasis until death. Black circles label progression of local disease in the brain. Green indicates patients that stopped silibinin because they entered in a clinical trial. Asterisks indicate patients who received silibinin when under palliative care. Grey arrow indicates patients still alive. **g.** MRI of a patient treated with silibinin who progressed locally (red arrows) although remained without clinical symptoms derived from CNS disease. Newly emerged micro-metastases in the Cerebellum remained <1 cm and without associated edema. **h.** Overall response rate (ORR) waterfall plot from extracranial disease (primary tumors and extracranial metastases) in 15 out of the 18 patients with lung cancer metastatic to the brain that received silibinin. 3 excluded patients did not have extracranial disease (2) or target (measurable) lesion according to RECIST v1.1 criteria. Dotted grey line indicates 30% reduction.

ACKNOWLEDGEMENTS

We acknowledge members of CNIO Core Facilities for their assistance. We also thank F.X. Real, O. Marín, M. Serrano, O. Fernandez-Capetillo and M. Soengas for critically reading the manuscript, Héctor Peinado for B16/F10 cell line, Joan Massagué for BrM cell lines, MEDA for Legasil®.

This work was supported by MINECO grants MINECO-Retos SAF2014-57243-R (M.V.), MINECO-Europa Excelencia SAF2015-62547-ERC (M.V.), IX FERO Grant for Research in Oncology (M.V.), Melanoma Research Alliance Young Investigator Award 2017 (M.V.), SEOM (J.B.B.), Pfizer WI190764 (J.B.B.), Meda Pharma (J.B.B.), Armangué Family Fund (J.A.M., J.B.B.), La Caixa-Severo Ochoa International PhD Program Fellowship (L.Z.), FCT PhD Fellowship SFRH/BD/100089/2014 (C.M.). M.V.

is a Ramón y Cajal Investigator (RYC-2013-13365). Authors declare no financial interests in connection to this work.

Bibliography

1. Lee, H.-T. *et al.* Stat3 orchestrates interaction between endothelial and tumor cells and inhibition of Stat3 suppresses brain metastasis of breast cancer cells. *Oncotarget* **6,** 10016–10029 (2015).

2. Kong, L.-Y. *et al.* A novel inhibitor of signal transducers and activators of transcription 3 activation is efficacious against established central nervous system melanoma and inhibits regulatory T cells. *Clin Cancer Res* **14,** 5759–5768 (2008).

3. Hatiboglu, M. A. *et al.* The tumor microenvironment expression of p-STAT3 influences the efficacy of cyclophosphamide with WP1066 in murine melanoma models. *Int J Cancer* **131,** 8–17 (2012).

4. Ganat, Y. M. *et al.* Early postnatal astroglial cells produce multilineage precursors and neural stem cells in vivo. *J Neurosci* **26,** 8609–8621 (2006).

5. Alonzi, T. *et al.* Essential role of STAT3 in the control of the acute-phase response as revealed by inducible gene inactivation [correction of activation] in the liver. *Mol Cell Biol* **21,** 1621–1632 (2001).

6. Valiente, M. *et al.* Serpins promote cancer cell survival and vascular co-option in brain metastasis. *Cell* **156,** 1002–1016 (2014).

7. Singh, M. *et al.* STAT3 pathway regulates lung-derived brain metastasis initiating cell capacity through miR-21 activation. *Oncotarget* **6,** 27461–27477 (2015).

8. Okada, S. *et al.* Conditional ablation of Stat3 or Socs3 discloses a dual role for reactive astrocytes after spinal cord injury. *Nat Med* **12,** 829–834 (2006).

9. Wanner, I. B. *et al.* Glial scar borders are formed by newly proliferated, elongated astrocytes that interact to corral inflammatory and fibrotic cells via STAT3-dependent mechanisms after spinal cord injury. *J Neurosci* **33,** 12870–12886 (2013).

10. LeComte, M. D., Shimada, I. S., Sherwin, C. & Spees, J. L. Notch1-STAT3-ETBR signaling axis controls reactive astrocyte proliferation after brain injury. *Proc Natl Acad Sci U S A* **112,** 8726–8731 (2015).

11. Ben Haim, L. *et al.* The JAK/STAT3 pathway is a common inducer of astrocyte reactivity in Alzheimer's and Huntington's diseases. *J Neurosci* **35,** 2817–2829 (2015).

12. Jee, Y., Kim, G., Tanuma, N. & Matsumoto, Y. STAT expression and localization in the central nervous system during autoimmune encephalomyelitis in Lewis rats. *J Neuroimmunol* **114,** 40–47 (2001).

13. Bachoo, R. M. *et al.* Epidermal growth factor receptor and Ink4a/Arf: convergent mechanisms governing terminal differentiation and transformation along the neural stem cell to astrocyte axis. *Cancer Cell* **1,** 269–277 (2002).

14. Anderson, M. A. *et al.* Astrocyte scar formation aids central nervous system axon regeneration. *Nature* **532,** 195–200 (2016).

15. Chen, Q. *et al.* Carcinoma-astrocyte gap junctions promote brain metastasis by cGAMP transfer. *Nature* **533,** 493–498 (2016).

16. Anderson, M. A., Ao, Y. & Sofroniew, M. V. Heterogeneity of reactive astrocytes. *Neurosci Lett* **565,** 23–29 (2014).

17. Berghoff, A. S. *et al.* Density of tumor-infiltrating lymphocytes correlates with extent of brain edema and overall survival time in patients with brain metastases. *Oncoimmunology* **5,** e1057388 (2016).

18. Jones, L. M. *et al.* STAT3 Establishes an Immunosuppressive Microenvironment during the Early Stages of Breast Carcinogenesis to Promote Tumor Growth and Metastasis. *Cancer Res* **76,** 1416–1428 (2016).

19. Wang, T. *et al.* Regulation of the innate and adaptive immune responses by Stat-3 signaling in tumor cells. *Nat Med* **10,** 48–54 (2004).

20. Drukker, M. & Benvenisty, N. The immunogenicity of human embryonic stem-derived cells. *Trends Biotechnol* **22,** 136–141 (2004).

21. Aurora, A. B. & Olson, E. N. Immune modulation of stem cells and regeneration. *Cell Stem Cell* **15,** 14–25 (2014).

22. Dubeykovskaya, Z. *et al.* Neural innervation stimulates splenic TFF2 to arrest myeloid cell expansion and cancer. *Nat Commun* **7,** 10517 (2016).

23. Cho, J.-H. *et al.* Unique features of naive CD8+ T cell activation by IL-2. *J Immunol* **191,** 5559–5573 (2013).

24. Rosenblum, M. D., Way, S. S. & Abbas, A. K. Regulatory T cell memory. *Nat Rev Immunol* **16,** 90–101 (2016).

25. Sevenich, L. *et al.* Analysis of tumour- and stroma-supplied proteolytic networks reveals a brain-metastasis-promoting role for cathepsin S. *Nat Cell Biol* **16,** 876–888 (2014).

26. Ghoochani, A. *et al.* MIF-CD74 signaling impedes microglial M1 polarization and facilitates brain tumorigenesis. *Oncogene* **35,** 6246–6261 (2016).

27. Bosch-Barrera, J. *et al.* Response of brain metastasis from lung cancer patients to an oral nutraceutical product containing silibinin. *Oncotarget* **7,** 32006–32014 (2016).

28. Lee, Y., Park, H. R., Chun, H. J. & Lee, J. silibinin prevents dopaminergic neuronal loss in a mouse model of Parkinson's disease via mitochondrial stabilization. *J Neurosci Res* **93,** 755–765 (2015).

29. Bosch-Barrera, J. & Menendez, J. A. silibinin and STAT3: A natural way of targeting transcription factors for cancer therapy. *Cancer Treat Rev* **41,** 540–546 (2015).

30. Sperduto, P. W. *et al.* Estimating Survival in Patients With Lung Cancer and Brain Metastases: An Update of the Graded Prognostic Assessment for Lung Cancer Using Molecular Markers (Lung-molGPA). *JAMA Oncology* **3,** 827–831

(2017).

31. Bos, P. D. *et al.* Genes that mediate breast cancer metastasis to the brain. *Nature* **459,** 1005–1009 (2009).

32. Nguyen, D. X. *et al.* WNT/TCF signaling through LEF1 and HOXB9 mediates lung adenocarcinoma metastasis. *Cell* **138,** 51–62 (2009).

33. Malladi, S. *et al.* Metastatic Latency and Immune Evasion through Autocrine Inhibition of WNT. *Cell* **165,** 45–60 (2016).

34. Campeau, E. *et al.* A versatile viral system for expression and depletion of proteins in mammalian cells. *PLoS ONE* **4,** e6529 (2009).

35. Schildge, S., Bohrer, C., Beck, K. & Schachtrup, C. Isolation and culture of mouse cortical astrocytes. *J Vis Exp* (2013). doi:10.3791/50079

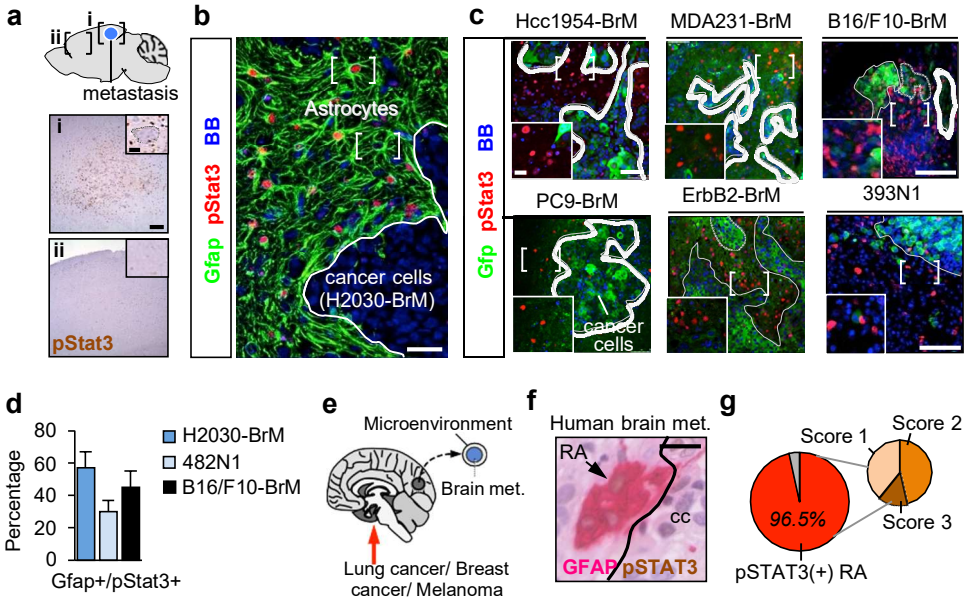
a
i
ii
metastasis
i
ii
pStat3
b
Gfap pStat3 BB
Astrocytes
cancer cells
(H2030-BrM)
c
Hcc1954-BrM
MDA231-BrM
B16/F10-BrM
Gfp pStat3 BB
PC9-BrM
ErbB2-BrM
393N1
cancer cells
d
Percentage
80
60
40
20
0
H2030-BrM
482N1
B16/F10-BrM
Gfap+/pStat3+
e
Microenvironment
Brain met.
Lung cancer/ Breast
cancer/ Melanoma
f
Human brain met.
RA
cc
GFAP pSTAT3
g
Score 1
Score 2
Score 3
96.5%
pSTAT3(+) RA
h
STAT3LOW RA
STAT3HIGH RA
OS (months)
100
80
60
40
20
0
P=0.0125
40
80
120
i
STAT3LOW cancer cells
STAT3HIGH cancer cells
OS (months)
100
80
60
40
20
0
P=0.9708
40
80
120

Figure 1

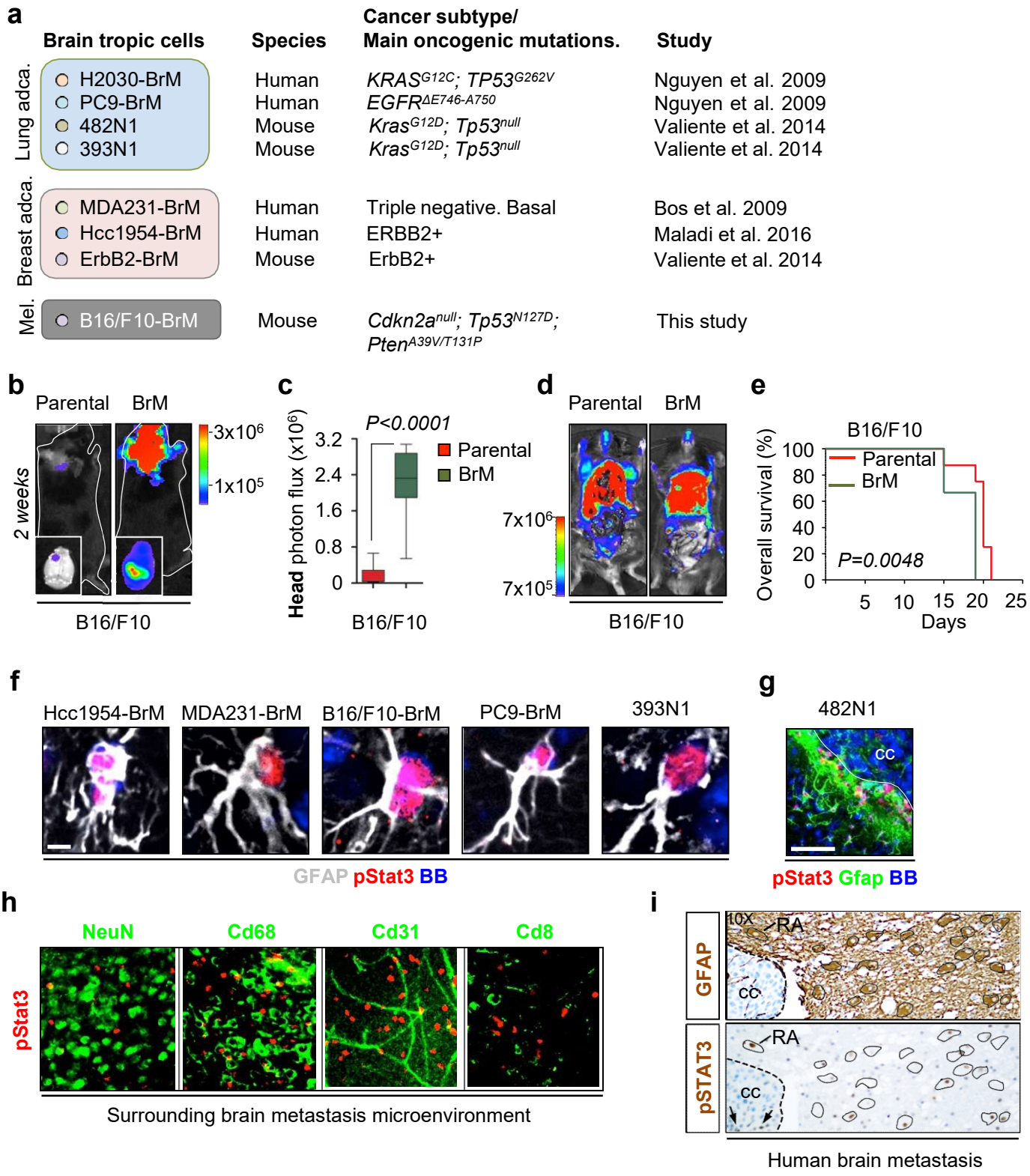
a
Brain tropic cells
Species
Cancer subtype/ Main oncogenic mutations.
Study
Lung adca.
H2030-BrM
PC9-BrM
482N1
393N1
Human
Human
Mouse
Mouse
KRASG12C; TP53G262V
EGFRΔE746-A750
KrasG12D; Tp53null
KrasG12D; Tp53null
Nguyen et al. 2009
Nguyen et al. 2009
Valiente et al. 2014
Valiente et al. 2014
Breast adca.
MDA231-BrM
Hcc1954-BrM
ErbB2-BrM
Human
Human
Mouse
Triple negative. Basal
ERBB2+
ErbB2+
Bos et al. 2009
Maladi et al. 2016
Valiente et al. 2014
Mel.
B16/F10-BrM
Mouse
Cdkn2anull; Tp53N127D; PtenA39V/T131P
This study
b
Parental
BrM
2 weeks
3x10^6
1x10^5
B16/F10
c
P<0.0001
Head photon flux (x10^6)
3.2
2.4
1.6
0.8
0
Parental
BrM
B16/F10
d
Parental
BrM
7x10^6
7x10^5
B16/F10
e
B16/F10
Overall survival (%)
100
80
60
40
20
0
Parental
BrM
P=0.0048
5
10
15
20
25
Days
f
Hcc1954-BrM
MDA231-BrM
B16/F10-BrM
PC9-BrM
393N1
GFAP pStat3 BB
g
482N1
cc
pStat3 Gfap BB
h
NeuN
Cd68
Cd31
Cd8
pStat3
Surrounding brain metastasis microenvironment
i
GFAP
10X
RA
cc
pSTAT3
RA
cc
Human brain metastasis

Figure S1

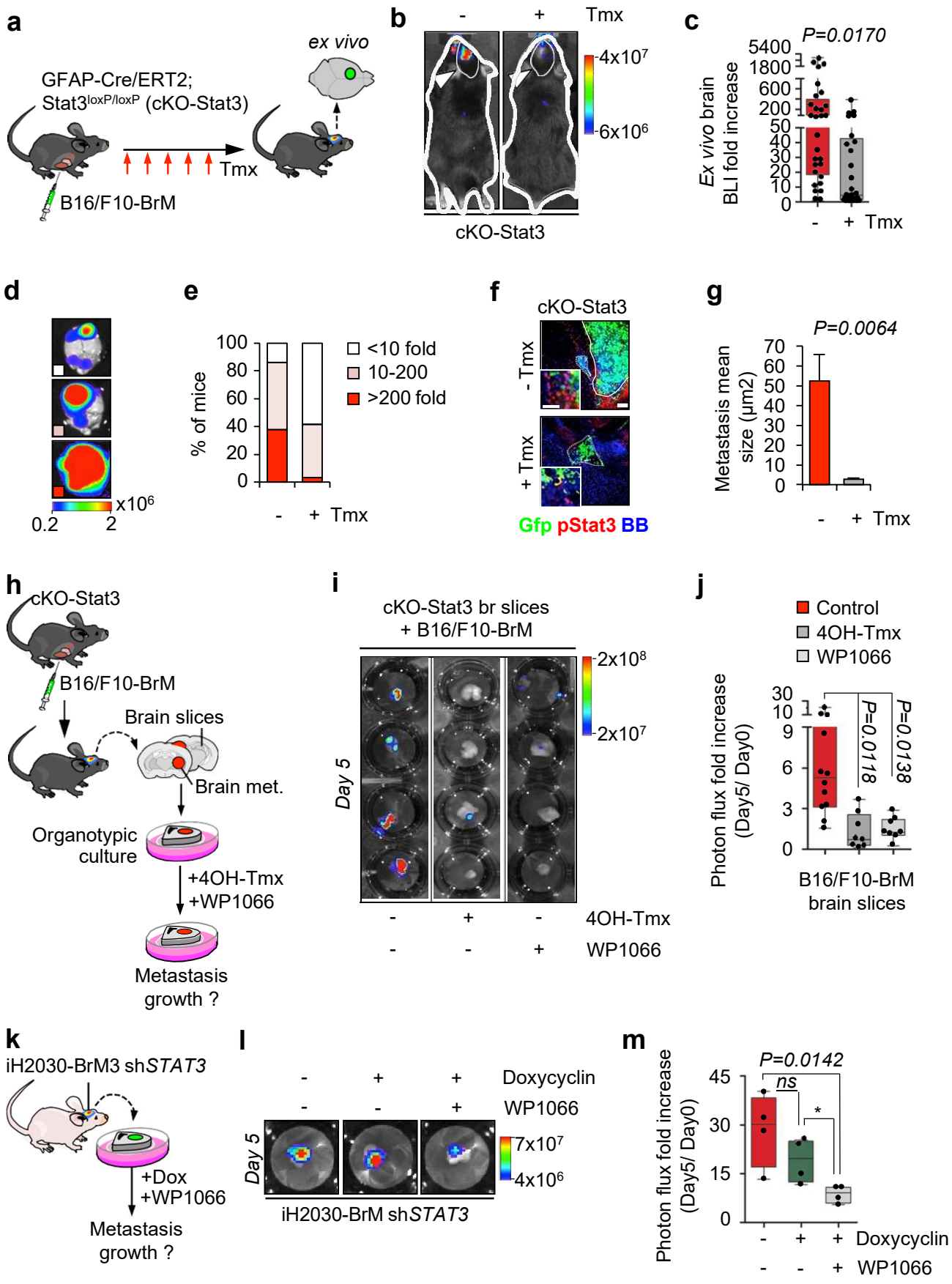
a
GFAP-Cre/ERT2;
Stat3loxP/loxP (cKO-Stat3)
Tmx
B16/F10-BrM
ex vivo
b
- + Tmx
4x10^7
6x10^6
cKO-Stat3
c
P=0.0170
Ex vivo brain BLI fold increase
5400
1800
600
200
50
40
30
20
10
0
- + Tmx
d
x10^6
0.2 2
e
% of mice
100
80
60
40
20
0
<10 fold
10-200
>200 fold
- + Tmx
f
cKO-Stat3
- Tmx
+ Tmx
Gfp pStat3 BB
g
P=0.0064
Metastasis mean size (µm2)
70
60
50
40
30
20
10
0
- + Tmx
h
cKO-Stat3
B16/F10-BrM
Brain slices
Brain met.
Organotypic culture
+4OH-Tmx
+WP1066
Metastasis growth ?
i
cKO-Stat3 br slices
+ B16/F10-BrM
2x10^8
2x10^7
Day 5
- + - 4OH-Tmx
- - + WP1066
j
Control
4OH-Tmx
WP1066
Photon flux fold increase (Day5/ Day0)
30
10
9
6
3
0
P=0.0118
P=0.0138
B16/F10-BrM brain slices
k
iH2030-BrM3 shSTAT3
+Dox
+WP1066
Metastasis growth ?
l
- + + Doxycyclin
- - + WP1066
Day 5
7x10^7
4x10^6
iH2030-BrM shSTAT3
m
P=0.0142
ns
*
Photon flux fold increase (Day5/ Day0)
45
30
15
0
- + + Doxycyclin
- - + WP1066

Figure 2

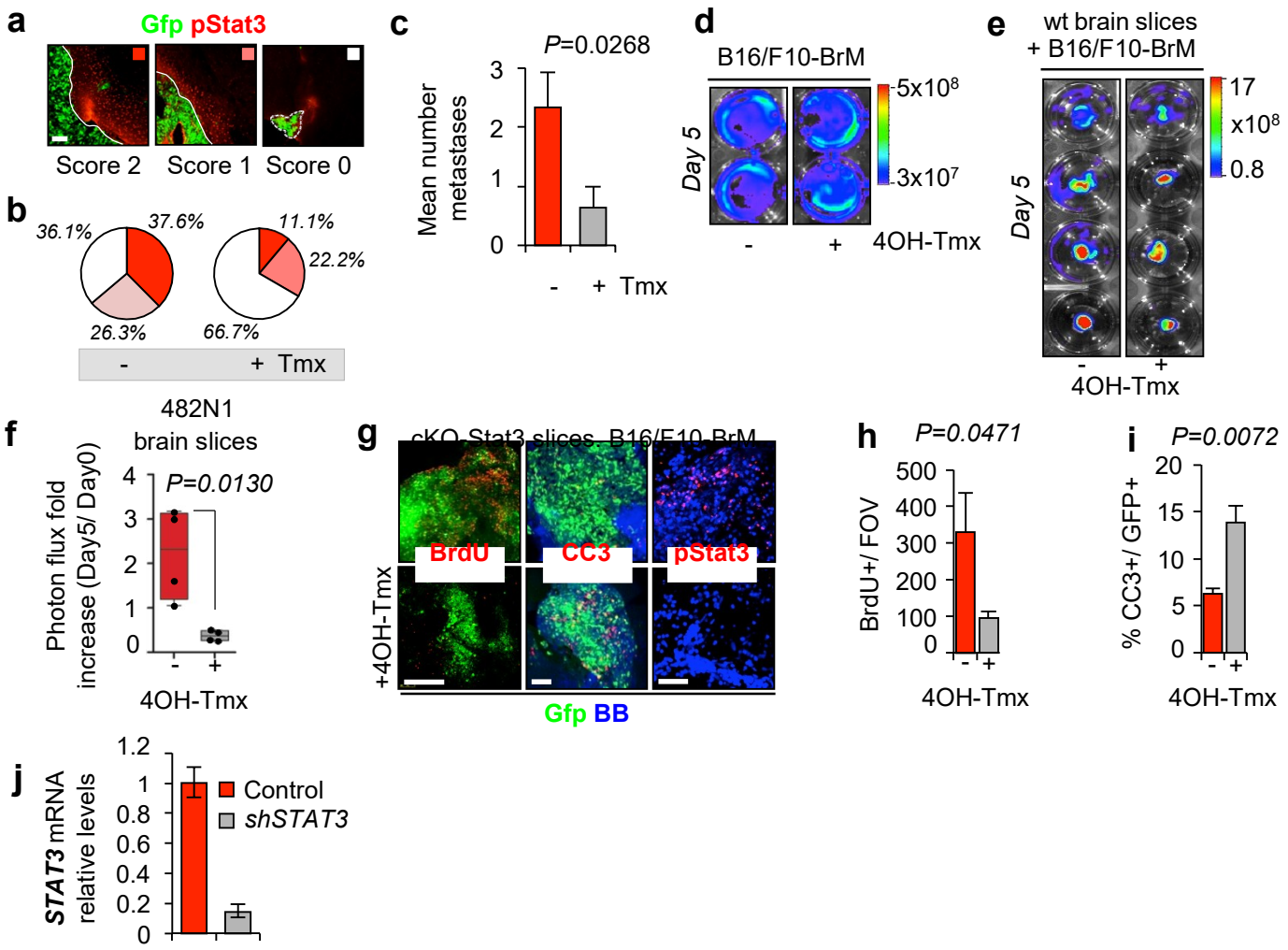
a
Gfp pStat3
Score 2
Score 1
Score 0
b
36.1%
37.6%
26.3%
11.1%
22.2%
66.7%
- + Tmx
c
P=0.0268
Mean number metastases
3
2
1
0
- + Tmx
d
B16/F10-BrM
Day 5
5x10^8
3x10^7
- + 4OH-Tmx
e
wt brain slices
+ B16/F10-BrM
Day 5
17
x10^8
0.8
- +
4OH-Tmx
f
482N1
brain slices
Photon flux fold increase (Day5/ Day0)
P=0.0130
4
3
2
1
0
- +
4OH-Tmx
g
cKO Stat3 slices B16/F10-BrM
BrdU
CC3
pStat3
+4OH-Tmx
Gfp BB
h
P=0.0471
BrdU+/ FOV
500
400
300
200
100
0
- +
4OH-Tmx
i
P=0.0072
% CC3+/ GFP+
20
15
10
5
0
- +
4OH-Tmx
j
STAT3 mRNA relative levels
1.2
1
0.8
0.6
0.4
0.2
0
Control
shSTAT3

Figure S2

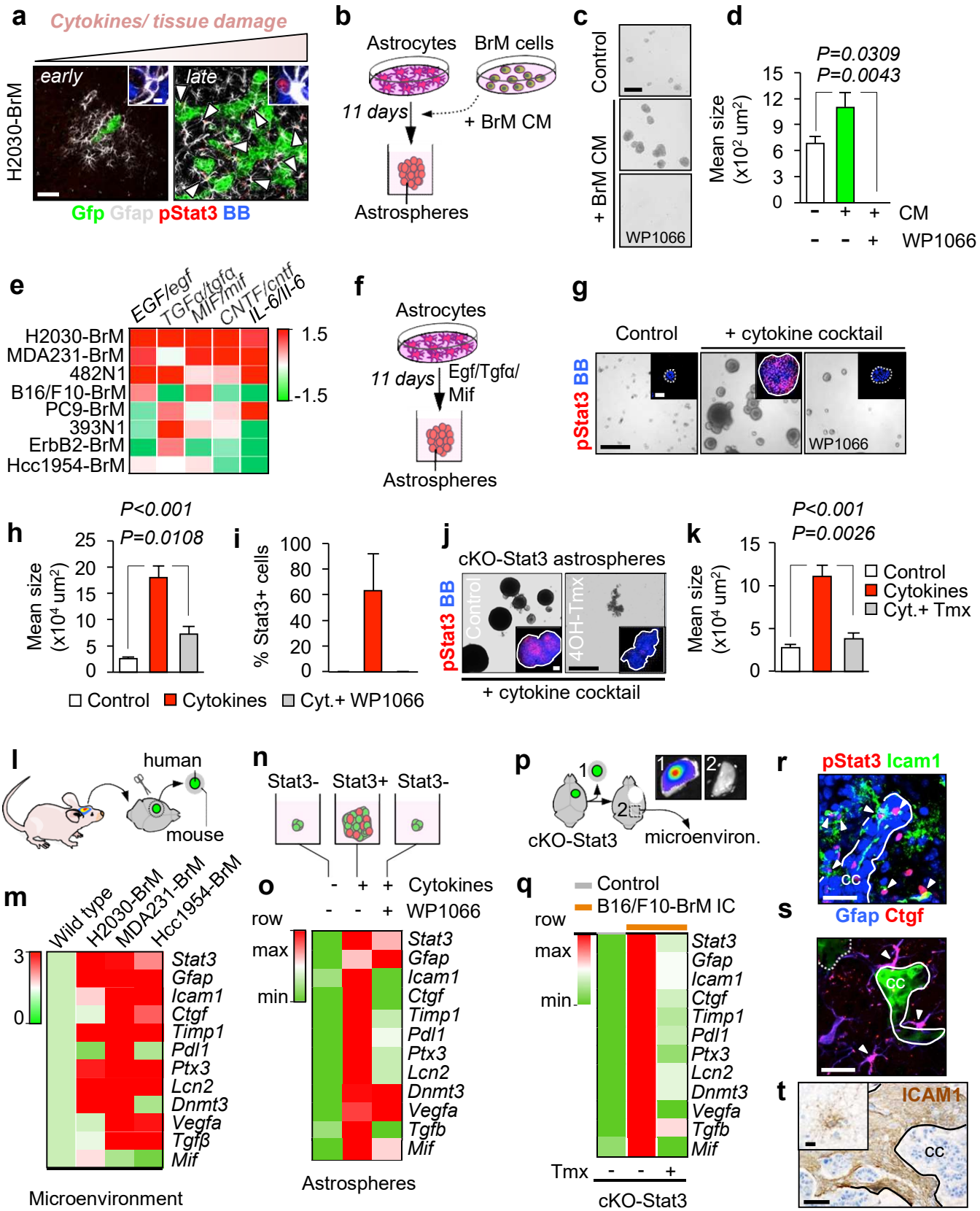
a
Cytokines/ tissue damage
H2030-BrM
early
late
Gfp Gfap pStat3 BB
b
Astrocytes
BrM cells
11 days
+ BrM CM
Astrospheres
c
Control
+ BrM CM
WP1066
d
P=0.0309
P=0.0043
Mean size (x10² um²)
CM
WP1066
e
EGF/egf
TGFα/tgfa
MIF/mif
CNTF/cntf
IL-6/Il-6
H2030-BrM
MDA231-BrM
482N1
B16/F10-BrM
PC9-BrM
393N1
ErbB2-BrM
Hcc1954-BrM
1.5
-1.5
f
Astrocytes
11 days
Egf/Tgfα/ Mif
Astrospheres
g
Control
+ cytokine cocktail
pStat3 BB
WP1066
h
P<0.001
P=0.0108
Mean size (x10⁴ um²)
Control
Cytokines
Cyt.+ WP1066
i
% Stat3+ cells
j
cKO-Stat3 astrospheres
pStat3 BB
Control
4OH-Tmx
+ cytokine cocktail
k
P<0.001
P=0.0026
Mean size (x10⁴ um²)
Control
Cytokines
Cyt.+ Tmx
l
human
mouse
m
Wild type
H2030-BrM
MDA231-BrM
Hcc1954-BrM
Stat3
Gfap
Icam1
Ctgf
Timp1
Pdl1
Ptx3
Lcn2
Dnmt3
Vegfa
Tgfβ
Mif
Microenvironment
n
Stat3-
Stat3+
Stat3-
o
Cytokines
WP1066
row
max
min
Astrospheres
p
cKO-Stat3
microenviron.
q
Control
B16/F10-BrM IC
Tmx
cKO-Stat3
r
pStat3 Icam1
cc
s
Gfap Ctgf
cc
t
ICAM1
cc

Figure 3

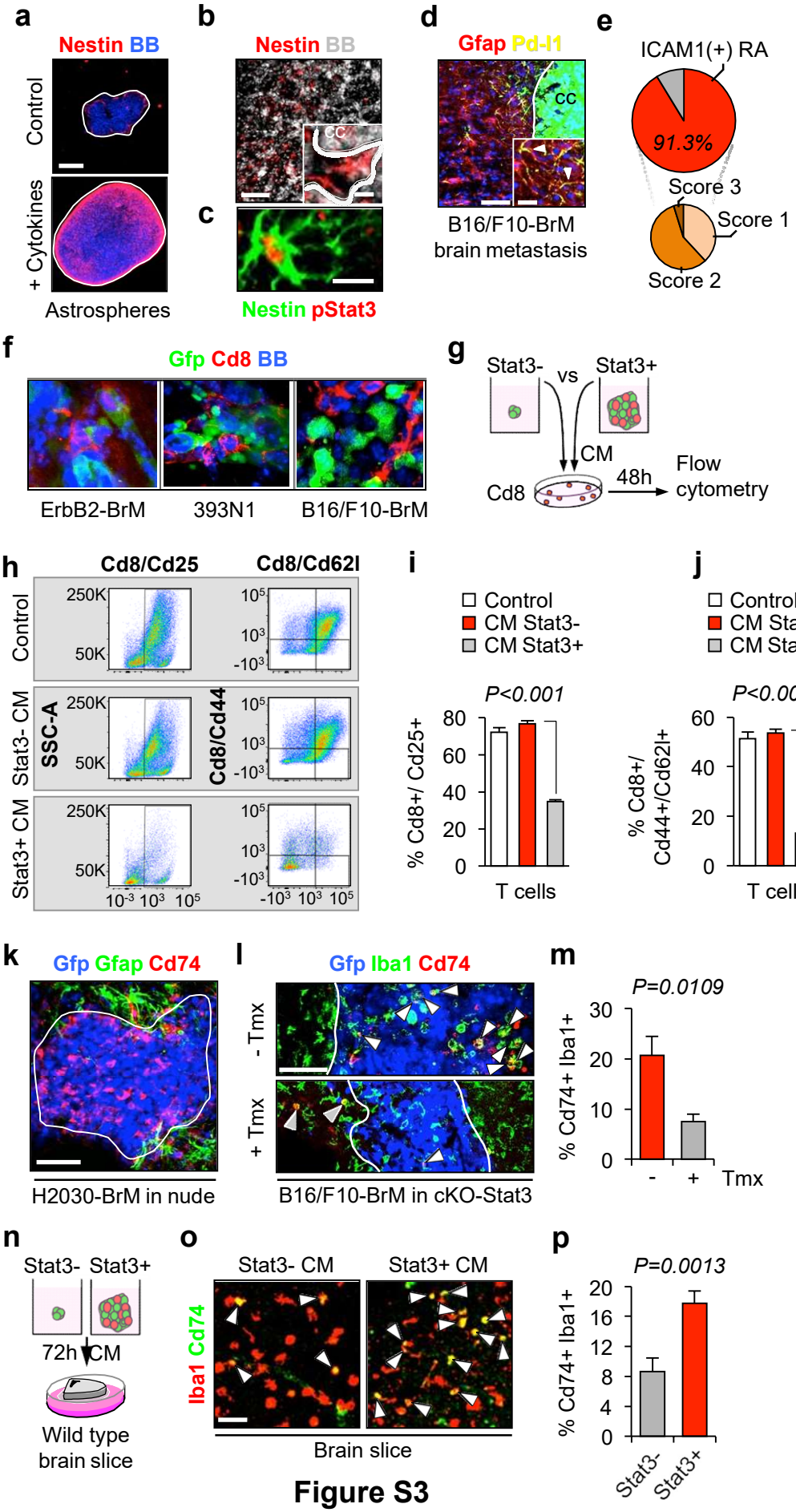
a
Nestin BB
Control
+ Cytokines
Astrospheres
b
Nestin BB
c
Nestin pStat3
d
Gfap Pd-l1
cc
B16/F10-BrM
brain metastasis
e
ICAM1(+) RA
91.3%
Score 3
Score 1
Score 2
f
Gfp Cd8 BB
ErbB2-BrM
393N1
B16/F10-BrM
g
Stat3-
vs
Stat3+
CM
Cd8
48h
Flow
cytometry
h
Cd8/Cd25
Cd8/Cd62l
Control
Stat3- CM
Stat3+ CM
SSC-A
Cd8/Cd44
250K
50K
i
Control
CM Stat3-
CM Stat3+
P<0.001
% Cd8+/ Cd25+
T cells
j
Control
CM Stat3-
CM Stat3+
P<0.001
% Cd8+/
Cd44+/Cd62l+
T cells
k
Gfp Gfap Cd74
H2030-BrM in nude
l
Gfp Iba1 Cd74
- Tmx
+ Tmx
B16/F10-BrM in cKO-Stat3
m
P=0.0109
% Cd74+ Iba1+
Tmx
n
Stat3-
Stat3+
72h CM
Wild type
brain slice
o
Stat3- CM
Stat3+ CM
Iba1 Cd74
Brain slice
p
P=0.0013
% Cd74+ Iba1+
Stat3-
Stat3+

Figure S3

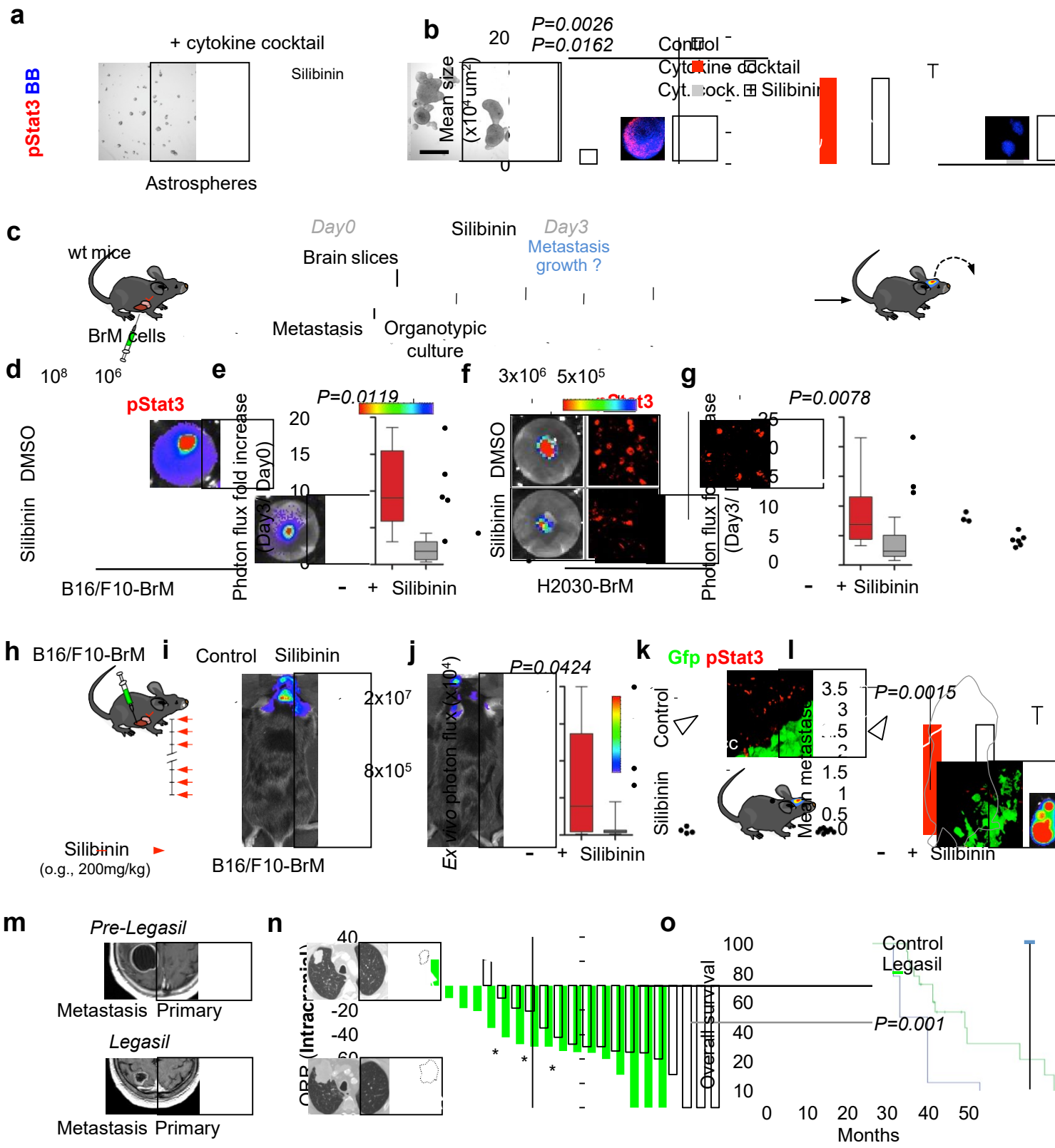
a
+ cytokine cocktail
Silibinin
pStat3 BB
Astrospheres
b
P=0.0026
P=0.0162
Control
Cytokine cocktail
Cyt. cock. + Silibinin
Mean size (x10⁴ um²)
c
wt mice
BrM cells
Day0
Brain slices
Silibinin
Day3
Metastasis growth ?
Metastasis
Organotypic culture
d
10⁸
10⁶
pStat3
DMSO
Silibinin
B16/F10-BrM
e
P=0.0119
Phdton flux fold increase (Day3/ Day0)
- + Silibinin
f
3x10⁶
5x10⁵
DMSO
Silibinin
H2030-BrM
g
P=0.0078
- + Silibinin
h
B16/F10-BrM
Silibinin
(o.g., 200mg/kg)
i
Control
Silibinin
2x10⁷
8x10⁵
B16/F10-BrM
j
P=0.0424
Ex vivo photon flux (x10⁴)
- + Silibinin
k
Gfp pStat3
Control
Silibinin
l
P=0.0015
Mean metastasis
- + Silibinin
m
Pre-Legasil
Metastasis Primary
Legasil
Metastasis Primary
n
ORR (Intracranial)
40
-20
-40
o
Overall survival
Control
Legasil
P=0.001
Months
0 10 20 30 40 50

Figure 4

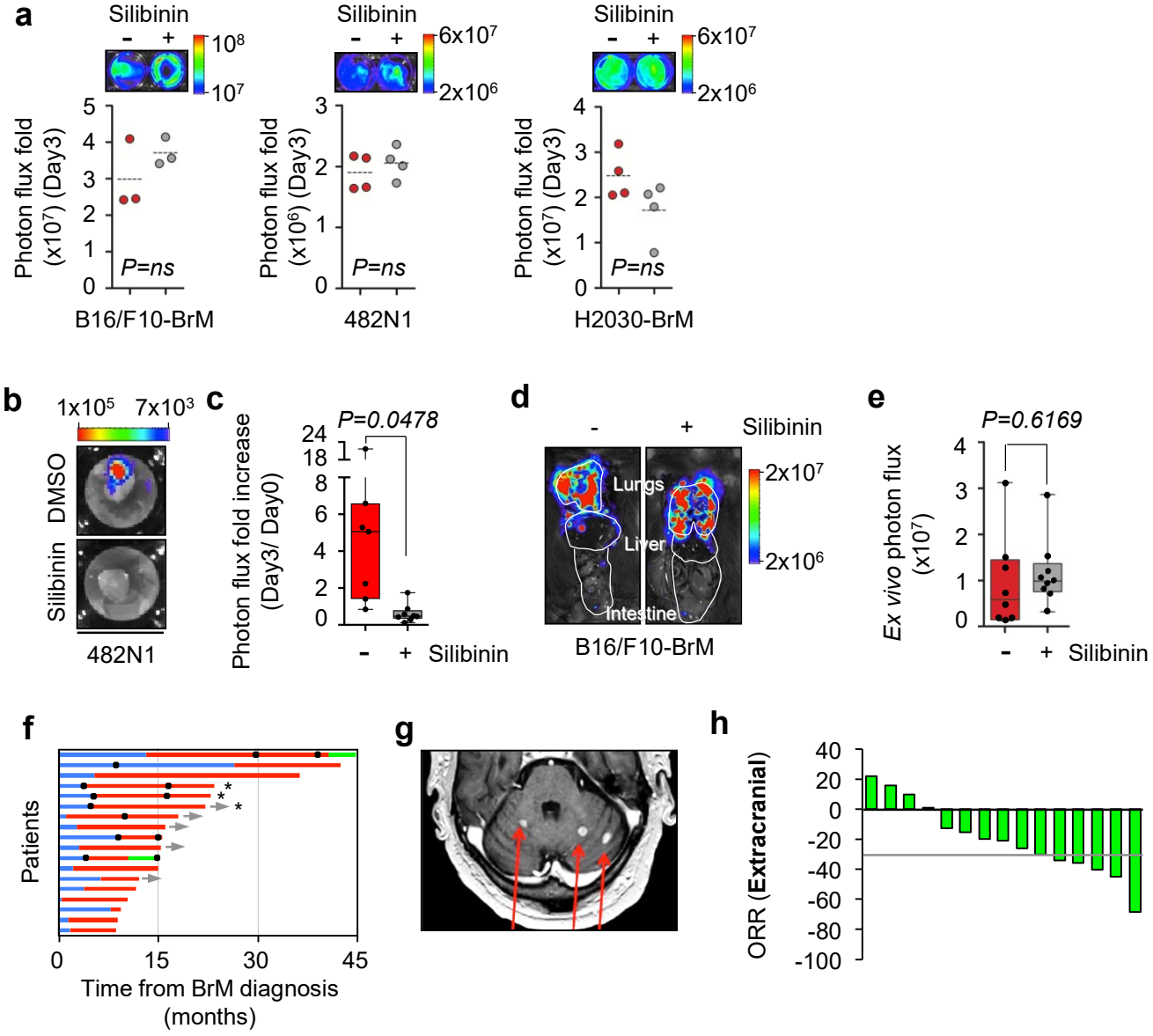
a
Silibinin
- +
10^8
10^7
Photon flux fold ($x10^7$) (Day3)
P=ns
B16/F10-BrM
Silibinin
- +
6x10^7
2x10^6
Photon flux fold ($x10^6$) (Day3)
P=ns
482N1
Silibinin
- +
6x10^7
2x10^6
Photon flux fold ($x10^7$) (Day3)
P=ns
H2030-BrM
b
1x10^5 7x10^3
DMSO
Silibinin
482N1
c
P=0.0478
Photon flux fold increase (Day3/ Day0)
- + Silibinin
d
- + Silibinin
Lungs
Liver
Intestine
2x10^7
2x10^6
B16/F10-BrM
e
P=0.6169
Ex vivo photon flux ($x10^7$)
- + Silibinin
f
Patients
Time from BrM diagnosis (months)
g
h
ORR (Extracranial)

Figure S4

Table 1
Brain metastasis samples analyzed for pStat3 in reactive astrocytes

Sample	1ry tumor	Subtype	Oncogenomics	pSTAT3 IHC in RA	Survival (from diagnosis) in months
#1	Lung	Adenocarcinoma	EGFR mutant exon 21 L858R	1	106
#2	Lung	Squamous cell carcinoma	ND	2	26
#3	Lung	squamous cell carcinoma	ND	2	34
#4	Lung	Adenocarcinoma	EGFRwt; ALKwt	2	27
#5	Lung	Adenocarcinoma	ALKwt	1	64
#6	Lung	Adenocarcinoma	ND	1	36
#7	Lung	Adenocarcinoma	ND	1	106
#8	Lung	Adenocarcinoma	ND	2	32
#9	Lung	Adenocarcinoma	ND	1	1
#10	Lung	Squamous cell carcinoma	ND	1	42
#11	Lung	Adenocarcinoma	ND	2	19
#12	Lung	Adenocarcinoma	ALKwt; ROSwt	2	
#13	Lung	Large cell neuroendocrine carcinom	EGFRwt; ALKwt; ROSwt	3	
#14	Lung	Adenocarcinoma	EGFRwt; ALKwt; ROSwt	2	
#15	Lung	Undifferentiated carcinoma	EGFRwt; ALKwt; ROSwt	3	
#16	Lung	Squamous	ND	2	
#17	Lung	Carcinoma	ND	2	
#18	Lung	Adenocarcinoma	EGFRwt; ALKwt; ROSwt	3	
#19	Lung	Non small cell lung cancer	EGFRwt; ALKwt; ROSwt	1	
#20	Lung	Adenocarcinoma	ND	1	50
#21	Lung	Adenocarcinoma	ND	2	13
#22	Breast	Lobular carcinoma	ND	2	
#23	Breast	Adenocarcinoma	HER2+; ER-; PR-	1	24
#24	Breast	Adenocarcinoma	ND	0	18
#25	Breast	Carcinoma	HER2+; ER+; PR-	2	
#26	Breast	Carcinoma	HER2+	3	
#27	Breast	Adenocarcinoma	ND	1	105
#28	Melanoma		BRAF wt	1	
#29	Melanoma		BRAF V600E	1	47

ND: Not determined

Table 2: Patient characteristics. Data are n (%). GPA=graded prognostic assessment. PS=performance status.

Sex	
Male	11 (61%)
Female	7 (39%)
Age	
<70 y	16 (89%)
>70 y	2 (11%)
Karnofsky PS	
>70%	8 (44%)
≤70%	10 (56%)
Extracraneal metastases	
Present	16 (89%)
Absent	2 (11%)
Histology	
Small cell	2 (11%)
Squamous	1 (5.5%)
Adenocarcinoma	14 (78%)
Large Cell	1 (5.5%)
Brain Metastases status	
Newly diagnosed	13 (72%)
Progressive disease	5 (28%)
GPA prognostic class	
3.5-4.0	0
2.5-3.0	1 (5.5%)
1.5-2.0	8 (44.5%)
0.0-1.0	9 (50%)
Gene status	
EGFR pos	4 (22%)
ALK pos	1 (5%)

Table 3. Systemic treatment administered to the patients. * Treatment received in a clinical trial, the patient stopped Silibinin supplementation before inclusion to the clinical trial and during all the treatment with this experimental drug according to study protocol.

First line	17 (95%)
Carboplatin-pemetrexed	6
Cisplatin-pemetrexed	2
Pemetrexed	2
Carboplatin-etoposide	2
EGFR TKI	4
Carboplatin-gemcitabine	1
Second line	13 (72%)
Carboplatin-pemetrexed	4
Pemetrexed	3
Docetaxel	2
Docetaxel-nintedanib	1
Nivolumab	1
Carboplatin-etoposide	1
Crizotinib	1
Third line	7 (39%)
Carboplatin-gemcitabine	2
Erlotinib	2
Docetaxel-nintedanib	1
3rd generation EGFR TKI*	1
3rd generation ALK TKI*	1
Fourth line	3 (17%)
Pemetrexed	1
Nivolumab	1
Erlotinib	1